Research Article

# Transcriptome analysis of molecular mechanisms underlying facial nerve injury repair in rats

https://doi.org/10.4103/1673-5374.310700

Date of submission: October 6, 2020

Date of decision: November 4, 2020

Date of acceptance: January 21, 2021

Date of web publication: March 25, 2021

Qian-Qian Cao[1, #], Shuo Li[2, #], Yan Lu[1], Di Wu[2], Wei Feng[1], Yong Shi[3, *], Lu-Ping Zhang[2, *]

**Graphical Abstract** *Transcriptome changes in the injured facial nerve trunk after facial nerve injury*

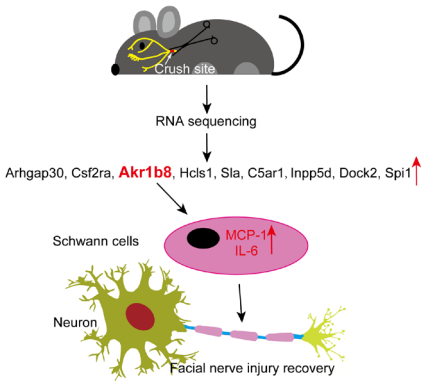


## Abstract

Although the transcriptional alterations inside the facial nucleus after facial nerve injury have been well studied, the gene expression changes in the facial nerve trunk after injury are still unknown. In this study, we established an adult rat model of facial nerve crush injury by compressing the right lateral extracranial nerve trunk. Transcriptome sequencing, differential gene expression analysis, and cluster analysis of the injured facial nerve trunk were performed, and 39 intersecting genes with significant variance in expression were identified. Gene Ontology annotation and Kyoto Encyclopedia of Genes and Genomes pathway analyses of the 39 intersecting genes revealed that these genes are mostly involved in leukocyte cell-cell adhesion and phagocytosis and have essential roles in regulating nerve repair. Quantitative real-time polymerase chain reaction assays were used to validate the expression of pivotal genes. Finally, nine pivotal genes that contribute to facial nerve recovery were identified, including *Arhgap30*, *Akr1b8*, *C5ar1*, *Csf2ra*, *Dock2*, *Hcls1*, *Inpp5d*, *Sla*, and *Spi1*. Primary Schwann cells were isolated from the sciatic nerve of neonatal rats. After knocking down *Akr1b8* in Schwann cells with an Akr1b8-specific small interfering RNA plasmid, expression levels of monocyte chemoattractant protein-1 and interleukin-6 were decreased, while cell proliferation and migration were not obviously altered. These findings suggest that *Akr1b8* likely regulates the interaction between Schwann cells and macrophages through regulation of cytokine expression to promote facial nerve regeneration. This study is the first to reveal a transcriptome change in the facial nerve trunk after facial nerve injury, thereby revealing the potential mechanism underlying repair of facial nerve injury. This study was approved by the Animal Ethics Committee of Nantong University, China in 2018 (approval No. S20180923-007).

**Key Words:** Akr1b8; cell proliferation; facial nerve injury; Gene-Act Networks; inflammatory response; RNA-Seq; Schwann cells; transcriptomics analysis

Chinese Library Classification No. R446; R745.1+2; R344+.13

## Introduction

In human beings, the face most effectively conveys expressions, and the facial nerve directly innervates facial expression muscles. The facial nerve is part of the peripheral nervous system (PNS), consisting of both motor and sensory components. Facial nerve injury, a common peripheral nerve injury, can be caused by a variety of factors and leads to loss of facial expression muscle function (Spencer and Irving, 2016). Without good recovery, facial nerve injury can induce disfigurement with cosmetic, functional, and psychological repercussions (Spencer and Irving, 2016). Although some facial nerve repair methods have been developed, including direct facial nerve anastomosis, nerve replacement, and nerve transplantation, the prognosis of facial nerve injury remains poor (Bíró, 2017; Gao et al., 2019). Thus, it is necessary to understand the mechanism underlying facial nerve injury to identify more effective therapeutic approaches for nerve injuries.

The sciatic nerve crush model has been widely applied to investigate the mechanism underlying peripheral nerve injury, and great progress has been accomplished (Cho et al., 2015; Gong et al., 2016; Weng et al., 2018; Caillaud et

[1]Key Laboratory of Neuroregeneration of Jiangsu and Ministry of Education, Co-innovation Center of Neuroregeneration, Nantong University, Nantong, Jiangsu Province, China; [2]Department of Otolaryngology, Affiliated Hospital of Nantong University, Nantong, Jiangsu Province, China; [3]Department of Otolaryngology, Head and Neck Surgery, Eye, Ear, Nose and Throat Hospital, Fudan University, Shanghai, China

***Correspondence to:** Lu-Ping Zhang, PhD, zhanglp910@126.com; Yong Shi, PhD, yongshifudan@126.com.

https://orcid.org/0000-0003-1745-081X (Lu-Ping Zhang); https://orcid.org/0000-0003-4139-0116 (Yong Shi)

#Both authors contributed equally to the work.

***How to cite this article:*** *Cao QQ, Li S, Lu Y, Wu D, Feng W, Shi Y, Zhang LP (2021) Transcriptome analysis of molecular mechanisms underlying facial nerve injury repair in rats. Neural Regen Res 16(11):2316-2323.*

al., 2019). Nerves in the PNS have an intrinsic capacity to regenerate after injury, in contrast to those in the central nervous system (Yu et al., 2011; He and Jin, 2016; Mahar and Cavalli, 2018). After peripheral nerve injury, injured neurons undergo many cellular and molecular changes involving processes, such as Wallerian degeneration, growth cone formation, mitochondrial transport, local axonal translation, and cytoskeletal remodeling, to promote intrinsic nerve regeneration and achieve successful functional recovery (He and Jin, 2016; Mahar and Cavalli, 2018). These changes are regulated by alteration of the expression of numerous genes (Christie and Zochodne, 2013; Chan et al., 2014). Our previous study using the sciatic nerve crush model identified multiple transcriptional alterations in the dorsal root ganglia after nerve injury (Gong et al., 2016). Several previous studies have identified the transcriptional program in the facial motor nucleus after facial nerve transection via microarray analysis (Zujovic et al., 2005; Stern et al., 2012; Gey et al., 2016). However, alteration of gene expression in peripheral nerves following facial nerve injury remains unknown. Therefore, an urgent need exists to understand the transcriptional changes of facial nerves after facial nerve injury from a global perspective to fully understand the mechanisms underlying nerve regeneration in the PNS.

Compared with cDNA microarrays, RNA sequencing (RNA-seq) is a more popular high-throughput technique for genome-wide transcriptome profiling. To fill the gap in facial nerve research, herein, we investigated the transcriptome changes and identified the key genes in nerve repair after facial nerve crush injury by RNA-seq. Schwann cells (SCs), infiltrating immune cells, and local axonal mRNA transport could contribute to these transcriptome changes in facial nerves following injury. Thus, we further employed SCs to preliminarily explore the functional role and potential mechanism of the identified key genes in facial nerve injury repair regulation. Collectively, the purpose of this study is to investigate transcriptome changes in the injured facial nerve trunk after facial nerve injury and provide potential mechanisms underlying facial nerve injury repair.

## Materials and Methods

### Animals

Sixty 6-week-old male Sprague-Dawley rats (specific pathogen-free level), weighing 160–180 g, were included in this study. Another six 1-day-old Sprague-Dawley rats (specific pathogen-free level) were used for SC analysis. All rats were obtained from the Experimental Animal Center of Nantong University (License No. SYXK (Su) 2014-0001 and SYXK (Su) 2017-0046). This study was approved by the Animal Ethics Committee of Nantong University of China (Approval No. S20180923-007) in 2018. All animal surgeries and experiments were carried out in accordance with the Administration Committee of Experimental Animals, Jiangsu Province, China. All experiments were designed and reported according to the Animal Research: Reporting of *In Vivo* Experiments (ARRIVE) guidelines. The breeding environment was as follows: temperature: 20–26°C, relative humidity: 40–70%, illumination: minimum working illumination ≥ 200 lx, animal illumination: 15–20°C, light/dark cycle: 12 hours/12 hours.

### Establishment of the facial nerve crush injury model

The facial nerve crush surgery was carried out in male rats as previously reported (Hadlock et al., 2005; Gao et al., 2019). All included rats were randomly divided into six groups ($n$ = 10). After the animals were anesthetized by intraperitoneal injection of anesthetics including 85 mg/kg trichloroacetaldehyde monohydrate (Lingfeng Chemical Reagent, Shanghai, China), 42 mg/kg magnesium sulfate (Lingfeng Chemical Reagent, Shanghai, China), and 17 mg/kg sodium pentobarbital (MilliporeSigma, Burlington, MA, USA), the main trunk of the right extracranial facial nerve was exposed. The unilateral facial nerve was clipped 5 mm from the styloid foramen with hemostatic forceps (Ryward, Shenzhen, China) three times for 10 seconds each. Three teeth of the hemostatic forceps were used; therefore, the maximum strength was used. The 5-mm proximal stump segments were separately collected at 0 and 6 hours and 1, 4, 7, and 14 days after facial nerve crush injury from the six groups. In the functional analysis of the facial nerve performed when establishing the facial nerve crush injury model, two time points (21 and 28 days) were added to evaluate long-term functional recovery.

### RNA-seq and analysis of the facial nerve stump segment

Total RNA was extracted with TRIzol (Sigma, San Francisco, CA, USA) from the facial nerve stump segments. TruSeq stranded total RNA with a Ribo-Zero Gold kit (Illumina, San Diego, CA, USA) was used to digest and fragment the RNA and remove ribosomal RNA. Transcriptome sequencing was performed as described previously (Gong et al., 2016). The levels of genes at 0 and 6 hours and 1, 4, 7, and 14 days after facial nerve injury were expressed as fragments per kb million reads. The thresholds of a $P$ value < 0.05 and fold change ≥ 2 (log2 ≥ 1) were used to define differentially expressed genes (DEGs). A Venn diagram was drawn using jvenn, which is an online tool for drawing Venn diagrams (http://jvenn.toulouse.inra.fr/). DEGs were further submitted to series test of cluster analysis and co-expression network analysis to select candidate genes with the most obvious expression. The series test of cluster analysis was performed using Stem software (http://www.cs.cmu.edu/~jernst/stem/), and the co-expression network analysis was performed using CytoScape software (https://cytoscape.org/) with bioinformatics assistance from Shanghai OE Biotech. Co., Ltd. (Shanghai, China). Then, these candidate genes were uploaded for gene enrichment analysis with the corresponding database (Gene Ontology (GO) enrichment: http://geneontology.org/; Kyoto Encyclopedia of Genes and Genomes (KEGG) enrichment: http://www.genome.jp/kegg/), and the PubMed database (https://www.ncbi.nlm.nih.gov/gene/) was used to screen genes related to cell proliferation, migration, apoptosis, and the cell cycle.

### Quantitative real-time PCR

Total RNA was isolated from collected facial nerve segments with the TRIzol reagent. RNase-free DNase I and the PrimeScript RT reagent kit (TaKaRa, Dalian, China) were used to treat and reverse transcribe the isolated RNA. Quantitative real-time PCR (qRT-PCR) was performed with SYBR Premix Ex Taq (TaKaRa). GAPDH was used as an internal control to normalize mRNA expression. qRT-PCR was independently performed three times per sample, and the primers used are shown in **Additional Table 1**. The qRT-PCR parameters were as follows: 95°C for 5 minutes (stage 1); 95°C for 30 seconds and 60°C for 30 seconds (stage 2, 40 cycles); and 95°C for 15 seconds, 60°C for 1 minute, and 95°C for 15 seconds (stage 3). The expression levels of all mRNAs normalized to *GAPDH* were quantitatively analyzed according to the relative quantitation comparative Ct ($2^{-\Delta\Delta Ct}$) method.

### Scoring of facial nerve function

The function of the facial nerve was estimated and scored on three aspects (blink reflex, vibrissae movement, and tip position) according to a previously reported method (Gao et al., 2019). Briefly, the blink reflex was evaluated as follows: no distinction between the normal and injured sides was recorded as 0 points; delayed motion of the injured side was recorded as 1 point; and an unclosed eyelid on the injured side was recorded as 2 points. Vibrissae movement was evaluated as follows: no distinction between the normal and injured sides was recorded as 0 points; weak movement on

the injured side was recorded as 1 point; and disappearance of vibrissae movement on the injured side was recorded as 2 points. The tip position was evaluated as follows: positioning with the middle tip of the nose centered was recorded as 0 points, and a contralateral nose position was recorded as 1 point. Before surgery, complete and equal facial movement on both sides was observed in all animals. After surgical compression of the facial nerve, all animals were allowed to survive 30 days and were recorded by video (ONEPLUS A6000, Shenzhen, China). Video recordings of the blink reflex, vibrissae movement, and tip position were analyzed by two independent blinded observers at the time of acquisition. Each rat was evaluated independently. Average functional scores were calculated for the three categories. The total score was calculated as the sum of the three functional scores. A total score of 5 was considered to be a successful model of facial nerve injury. A higher score indicated more severe injury, and a lower score indicated a nearly normal condition.

**Isolation, culture, and transfection of primary SCs**

Primary SCs were isolated from the sciatic nerve according to a previously described method that is typically used to study the SC phenotype in facial nerves (Haastert et al., 2009; Yao et al., 2016; Gao et al., 2019). Briefly, 1-day-old rats (provided by the Experimental Animal Center of Nantong University) were sacrificed to provide sciatic nerve tissue to isolate primary SCs. Anti-Thy1.1 antibody (mouse, 1:1000, Cat# M7898, Sigma-Aldrich, St. Louis, MO, USA) and rabbit complement (25%, Cat# 31024100, Invitrogen, Carlsbad, CA, USA) were subsequently applied to remove fibroblasts and purify the isolated cells. Then, a specific SC marker (Yao et al., 2016), S100β (mouse, 1:1000, Cat# s2532, Sigma), was used to immunostain the purified cell preparation, and the results indicated that the cell preparation consisted of 98% SCs. The obtained SCs were maintained in Dulbecco's modified Eagle medium (Gibco, Grand Island, NY, USA) containing 10% fetal bovine serum (Gibco). SCs were passaged for less than three times before subsequent use.

Primary cultured SCs were transfected with negative-control small interfering RNA (siRNA) or Akr1b8-specific siRNA (Ribobio, Guangzhou, China) using the Lipofectamine RNAiMAX transfection reagent (Invitrogen). The target sequences of siRNA duplexes were as follows: negative-control siRNA, 5′-GGC UCU AGA AAA GCC UAU GC-3′, Akr1b8-specific siRNA-1, 5′-CTG GGT ATC GAC ATA TTG A-3′, Akr1b8-specific siRNA-2, 5′-ACC CTT CAC TAT TAC AGG A-3′, Akr1b8-specific siRNA-3, 5′-CAG CAC GTA TAC AGG AGA A-3′.

**5-Ethynyl-20-deoxyuridine proliferation assay**

At 2 days after transfection, the SCs were subjected to proliferation analysis. SC proliferation was detected with a 5-ethynyl-20-deoxyuridine (EdU) Cell Proliferation Kit (Ribobio) according to the manufacturer's instructions. For the EdU assay, the SCs were seeded at a density of $1 \times 10^5$ cells/well into a 96-well culture plate. Then, the seeded SCs were incubated with 50 μM EdU for 4 hours. Afterward, 4% paraformaldehyde was used to fix the SCs for 30 minutes, and Triton X-100 was subsequently applied to permeabilize the cells for 15 minutes. Finally, Apollo fluorescent dyes and 5 μg/mL Hoechst 33342 (Ribobio) were respectively used to stain the SCs and cell nuclei for 20 minutes. Four random areas per well of the stained SCs were imaged by an Olympus Corporation fluorescence microscope (Shinjuku, Tokyo, Japan). Each sample was replicated in three wells. Finally, ImageJ Software (National Institutes of Health, Bethesda, MD, USA) was applied for cell counting and analyses.

**Wound healing assay**

The wound healing assay was carried out in Culture-Insert 2 Wells in a 35-mm μ-Dish (iBidi, Martin Reid, Gräfelfing, Germany). For the wound healing assay, the Culture-Inserts were seeded on a six-well plate, and then SCs transfected with the indicated siRNAs were seeded in the two wells of the Culture-Insert. The seeded SCs were incubated for 24 hours to form a tight cell monolayer on the bottom of the six-well plate. Afterward, the Culture-Insert was removed to expose the area between the two wells, and then the clear area was photographed as a control (0 hours). The remaining cells were then starved in Dulbecco's modified Eagle medium with 5% fetal bovine serum and 0.15 μg/mL mitomycin C (Sigma) for 12 hours. Finally, migrating cells at the wound front were photographed, and the clear areas were measured by ImageJ software at the indicated time points to determine the percentage relative to that at 0 hours.

**Statistical analysis**

All statistical analyses were conducted by Student's *t*-test using GraphPad Prism 9 (GraphPad Software, San Diego, CA, USA). The DEGs were statistically analyzed using DESeq software (https://www.huber.embl.de/users/anders/DESeq/). A $P$-value < 0.05 was considered statistically significant, and all results are expressed as the mean ± standard deviation (SD).

## Results

**Establishment and evaluation of the facial nerve injury model**

To fully understand the transcriptome changes after facial nerve injury, we first established a facial nerve crush model and harvested the injured facial nerve trunk from rats at 0 and 6 hours and 1, 4, 7, and 14 days after surgery (**Figure 1A**). Thus, we estimated the three functional aspects (blink reflex, vibrissae movement, and tip position) of the facial nerve to test the effectiveness of the model. As shown in **Figure 1B**, compared with the pre-surgery condition, the tip position scores were significantly increased at 6 hours post-injury and gradually decreased to a normal level at 28 days post-injury. Meanwhile, the vibrissae movement and blink reflex scores were also increased at 6 hours post-injury (**Figure 1C** and **D**). Collectively, the total neurological scores were increased and indicated a serious facial nerve injury (**Figure 1E**). Taken together, the results indicate that our facial nerve crush model was well established.

**Identification of DEGs in the facial nerve crush injury model**

As shown in **Figure 1A**, the total RNA of facial nerve tissues was isolated and then subjected to deep sequencing. Mapping of the sequencing read alignment to the reference genome and genes suggested good sequence quality (**Additional Tables 2** and **3**). To screen out the most representative gene group for facial nerve repair, we performed a series test of cluster analysis to characterize the gene expression profile of the sequencing data. During the series test of cluster analysis, genes with the same change characteristics were clustered in a single expression pattern, and we finally identified 12 expression patterns for facial nerve tissues (**Additional Figure 1A**). Two of the 12 significant expression patterns were the most representative. Profile 9 was first down-regulated and then up-regulated compared with the control during the 14 days after injury, and the genes in profile 9 were highly involved in myelination, which is down-regulated at the initiation of axonal degeneration and up-regulated during late axon regeneration (**Additional Figure 1A** and **B**). Conversely, profile 48 was first up-regulated and then down-regulated, and the genes in profile 48 mainly participate in inflammatory and immune responses, which play important roles in early regeneration after peripheral nerve injury (**Figure 2A** and **B**). Here, we concentrated on the 299 genes in profile 48 and the initiation of facial nerve regeneration. By comparison with the RNA-seq

data at 0 hours after nerve injury, we identified 1120, 1166, 1312, 1210, and 1126 DEGs at 6 hours and 1, 4, 7, and 14 days post-nerve injury, respectively (**Figure 2C** and **Additional Table 4**). When the DEGs were analyzed at different time points, 246 genes were constitutively identified at all time points (**Figure 2C**). To further identify potential positive regulators of facial nerve recovery, we then compared the 299 genes in profile 48 with the 246 DEGs and identified 39 intersecting genes (**Figure 2D**). In conclusion, these data revealed that 39 genes showed significant expression, and most of them were first up-regulated and then down-regulated during facial nerve crush injury, suggesting that these genes may play an indispensable role in facial nerve injury repair.

**Functional enrichment analysis of specific DEGs**

The transcription levels of the 39 genes were first up-regulated at 6 hours post-injury and then down-regulated at 7 days post-injury (**Figure 3A**). To further investigate the expression and function of these 39 genes, we performed GO enrichment and KEGG pathway analyses. As shown in **Figure 3B**, categories such as leukocyte cell–cell adhesion and phagocytosis were significantly enriched. Furthermore, GO annotation also revealed the cellular components and molecular function of these 39 genes. These genes were mostly located on the cell surface and cellular membrane, while their molecular functions were related to protein kinase and protein binding (**Figure 3B**). Key signaling pathways elucidated by KEGG pathway analysis showed that phagosomes were obviously enriched (**Figure 3C**). Unexpectedly, we also found that some pathways related to bacterial or viral infection were enriched. However, the animals that we used were healthy, and all animal experiments were conducted within sterile barriers. Moreover, several genes in these infection-associated pathways, such as *C3*, *C5a*, and Toll-like receptor 2 (**Additional Table 5**) have been previously shown to play important roles in nerve regeneration (Dubový et al., 2013). A possible explanation for this phenomenon is that these genes are multifunctional and participate in the regulation of multiple signaling pathways. Next, we performed Gene-Act Network analysis based on the KEGG database to screen key genes. The interactions among the 39 key genes are shown in **Figure 3D** and **Additional Table 6**. Therefore, the bioinformatics analysis in this study offers functional insight into these 39 genes and highlights potential aspects for further exploration.

**qRT-PCR validation of key genes in Gene-Act Networks**

After biological analysis, qRT-PCR was performed to further verify the RNA-seq results for key genes. Degrees within the Gene-Act Networks represent the number of other genes regulated by a single gene, and a higher degree indicates a more central role of the single gene within the network. Therefore, we selected several key genes with a degree higher than 10 and estimated their RNA expression level throughout facial nerve injury (**Additional Table 6**). Consistently, the qRT-PCR results revealed that the transcription level of these genes was first up-regulated and then down-regulated, which was highly correlated with the RNA-seq data (**Figure 4A**). According to the RNA-seq data and the subsequent biological analysis and validation, we identified nine new genes, including *Arhgap30*, *Akr1b8*, *C5ar1*, *Csf2ra*, *Dock2*, *Hcls1*, *Inpp5d*, *Sla*, and *Spi1*, that may have pivotal roles in regulating facial nerve regeneration.

Among the nine genes, some have been previously validated to participate in cell proliferation, migration, apoptosis, or adhesion, including *Arhgap30*, *Akr1b8*, *Csf2ra*, and *Hcls1* (Shen et al., 2015; Mao and Tong, 2018; Arumugam et al., 2019; Aslam et al., 2019). Some of these genes are involved in the immune and inflammatory responses, such as *Akr1b8*, *Dock2*, *C5ar1*, *Inpp5d*, *Sla*, and *Spi1* (Dragone et al., 2006; Hamilton et al., 2011; Zhu et al., 2018; Li et al., 2019; Kunimura et al., 2020). It is well known that relevant biological processes play an important role in regulating nerve repair. The flexible differentiation state of PNS neurons and SCs contributes to the intrinsic regenerative capacity of peripheral nerves. SCs wrap around the axons of peripheral nerve fibers to form a myelin sheath and play a pivotal role in the regeneration of peripheral nerves (Yao et al., 2016). After nerve injury, SCs undergo dedifferentiation, proliferation, and migration, form bands of Bungner to provide guidance for regenerating axons, and secrete a variety of cytokines and neurotrophic factors to activate macrophages to engulf myelin fragments and support nerve regeneration (Hu et al., 2011; da Silva et al., 2014; Yao et al., 2016). Thus, we hypothesized that these indicated genes may play a crucial part in facial nerve injury repair by modulating SC phenotypes to promote proliferation, migration, adhesion, and inflammatory responses, but this requires further study (**Figure 4B**).

**Akr1b8 affects the synthesis of induced chemokines in SCs but does not affect SC proliferation and migration**

To preliminarily verify our hypothesis, we chose *Akr1b8* for further study. *Akr1b8*, Aldo-keto reductase 1B8, which functions in carbonyl detoxification and lipid biosynthesis, is a key protein in the proliferation and repair of colonic epithelial cells and plays a critical role in the pathogenesis of ulcerative colitis and colitis-associated colorectal cancer (Shen et al., 2015). However, it is currently unknown whether Akr1b8 plays a functional role in facial nerve repair. Previous studies have demonstrated that SCs play a crucial role in facial nerve regeneration (Rueger et al., 2008; Gao et al., 2019); thus, we chose SCs to explore the role of *Akr1b8* in facial nerve repair. To investigate whether *Akr1b8* has a direct effect on the phenotype of SCs, we designed three Akr1b8-specific siRNAs. *Akr1b8* was knocked down in SCs by transfection of cells with all three Akr1b8-specific siRNA plasmids (**Figure 5A**). We then chose the most effective Akr1b8-specific siRNA to silence *Akr1b8* in SCs and investigated the cell proliferation rate of these cells. To our surprise, the Edu assay used to analyze the rate of DNA synthesis revealed that *Akr1b8* knockdown had no effect on the cell proliferation rate of SCs (**Figure 5B** and **C**). The wound healing assay revealed that Akr1b8 also does not affect SC migration (**Figure 5D** and **E**).

After nerve injury, SCs not only proliferate and migrate but also produce inflammatory cytokines and chemokines for macrophage recruitment and myelin phagocytosis to repair injured nerves (Martini et al., 2008). Interleukin-6 (IL-6) participates in the neuronal and immune responses to injury, and its expression is upregulated in SCs after nerve transection (Tofaris et al., 2002). Monocyte chemoattractant protein-1 (MCP-1), another potential SC-derived macrophage attractant, is rapidly upregulated within 24 hours after sciatic nerve injury (Tofaris et al., 2002; Perrin et al., 2005). A previous study reported that *Akr1b8* may also affect pro-inflammatory cytokine expression (Shen et al., 2015). Thus, we further explored the effect of *Akr1b8* on inflammatory cytokine and chemokine expression in SCs. As shown in **Figure 5F** and **G**, compared with SCs transfected with negative-control siRNA, SCs transfected with the two effective Akr1b8-specific siRNAs presented significantly lower *IL-6* and *MCP-1* expression levels, indicating that *Akr1b8* knockdown disrupts the synthesis of inflammatory cytokines and chemokines in SCs. Collectively, these data suggest that *Akr1b8* may regulate facial nerve injury repair by modulating the synthesis of inflammatory cytokines rather than the proliferation and migration of SCs.

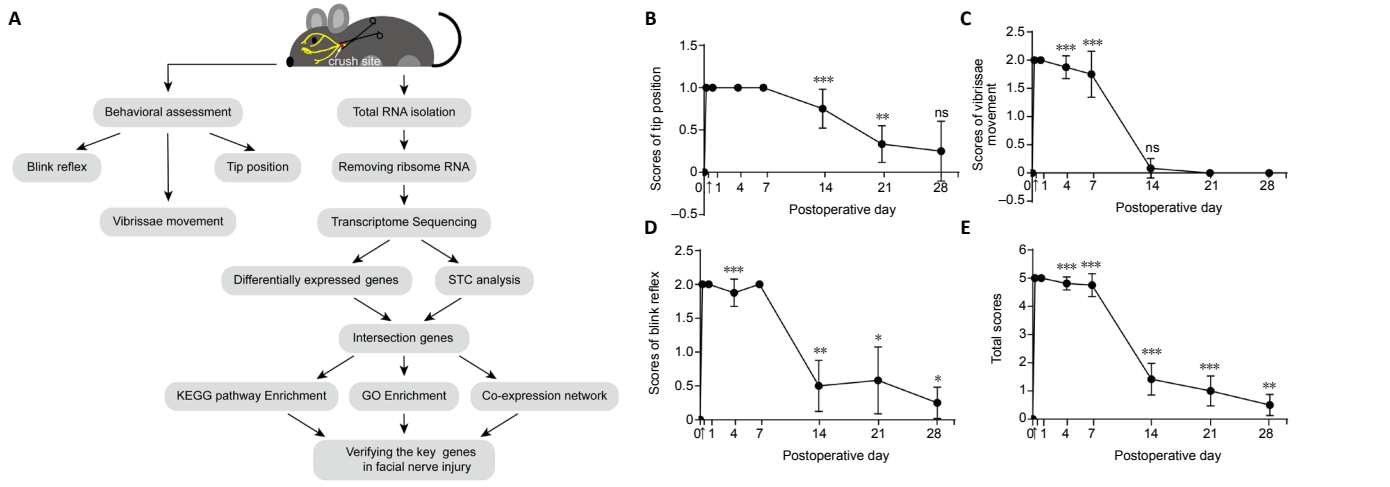


**Figure 1** | **Establishment of a facial nerve crush injury model.**
(A) Diagram of the transcriptome study of facial nerve injury. (B–E) Neurological scores at different times after facial nerve crush injury. All data are shown as the mean ± SD ($n$ = 8). *$P$ < 0.05, **$P$ < 0.01, ***$P$ < 0.001, *vs.* control group (0 hours) (Student's $t$-test). Accurate $P$-values for Figure 1B–E are listed in Additional Table 8. GO: Gene Ontology; KEGG: Kyoto Encyclopedia of Genes and Genomes; ns: non-significant; STC: series test of cluster.

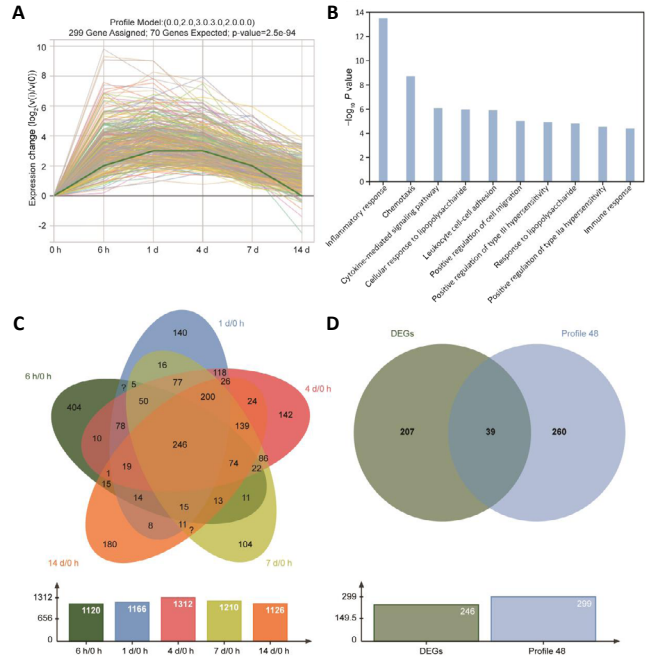


**Figure 2** | **DEG analysis in the facial nerve trunk following crush injury.**
(A) The detailed expression pattern of 299 genes in profile 9. All of the 299 genes were up-regulated at 6 hours post-injury and down-regulated from 4 to 7 days post-injury. (B) Biological process analysis of the 299 genes. (C) DEGs at different time points post-injury. The Venn diagram shows that a total of 246 genes were differentially expressed at all time points examined post-injury. (D) The intersection between DEGs and genes in profile 48. The Venn diagram shows that 39 genes were common to both the 246 DEGs and the 299 genes of profile 48. DEGs: Differentially expressed genes.

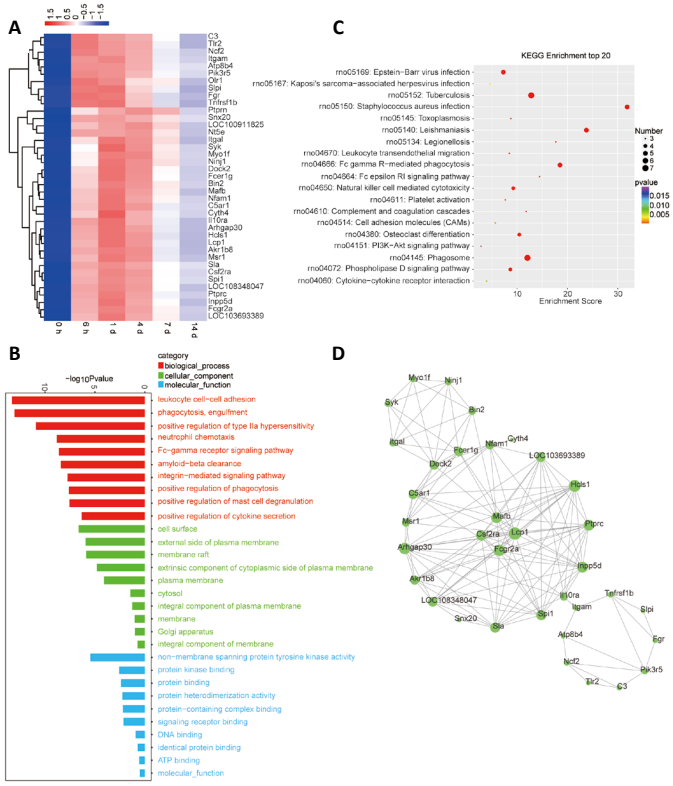


**Figure 3** | **Functional enrichment of the 39 specific differentially expressed genes in Figure 2D.**
(A) Heat map of expression levels of the 39 specific genes during the time course studied. The color scale shown on the top represents the relative expression level of the indicated genes: red indicates expression > 0, and blue indicates expression < 0. (B) GO enrichment analysis of the 39 specific genes. (C) Plot of KEGG enrichment of the significant pathways involving the 39 specific genes. The horizontal axis represents the enrichment score. The ordinate represents the functional description of the enriched pathway. A larger circle indicates that more genes were enriched for this function. The color spectrum ranging from blue to red represents the uncorrected $P$-value. (D) Co-expression network of the 39 specific genes. Cycle nodes in the network indicate genes, and edges between two nodes indicate interactions between genes. GO: Gene Ontology; KEGG: Kyoto Encyclopedia of Genes and Genomes.

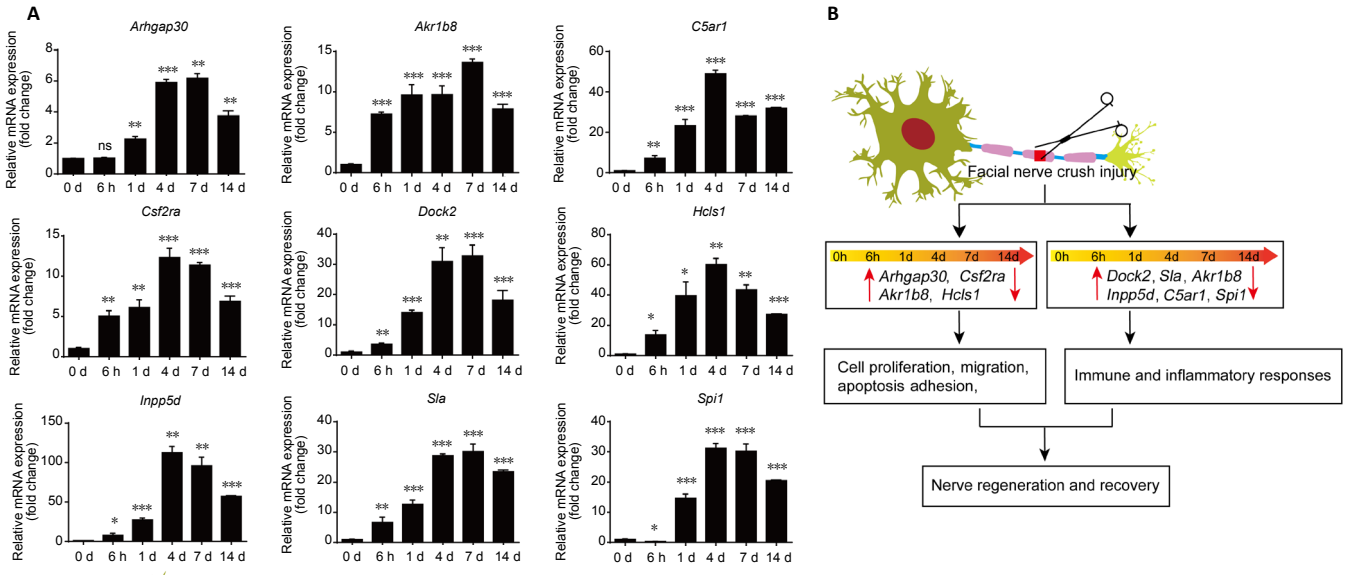


**Figure 4** | **Verification of expression of the key genes.**
(A) Quantitative reverse transcription-polymerase chain reaction estimation of mRNA expression of the indicated genes at different time points post-injury. All data are shown as the mean ± SD ($n$ = 3). *$P$ < 0.05, **$P$ < 0.01, ***$P$ < 0.001, *vs*. control group (0 hours) (Student's $t$-test). (B) Schematic diagram showing transcriptional changes at 14 days after facial nerve crush injury. The schematic diagram describes the nine key genes and their potential mechanisms of regulating facial nerve regeneration. ns: Non-significant.

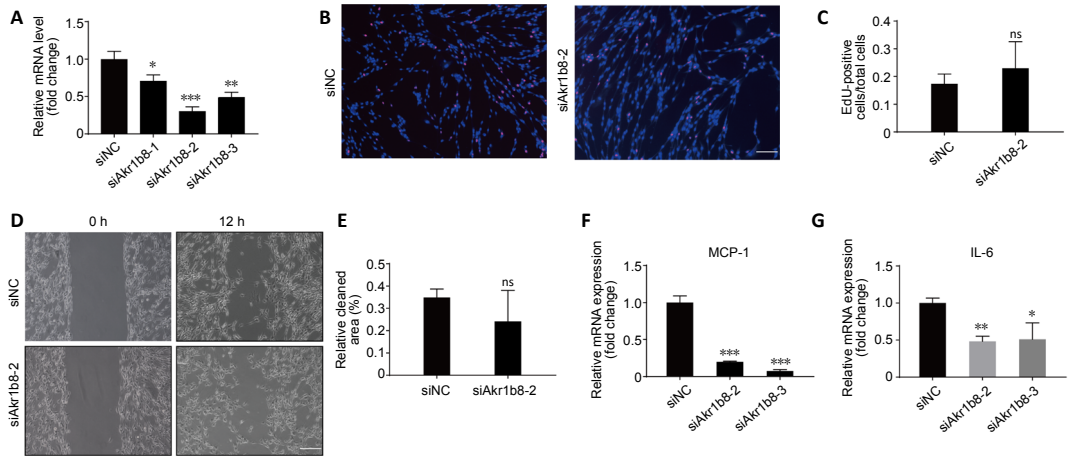


**Figure 5** | **The effect of *Akr1b8* knockdown on SC phenotype.**
(A) The mRNA expression level of Akr1b8 in SCs transfected with siNC or Akr1b8-specific siRNA (siAkr1b8-1, siAkr1b8-2, siAkr1b8-3) ($n$ = 3) (B, C) Effect of Akr1b8 knockdown on cell proliferation in SCs. (B) The cells were fluorescently stained with EdU (red), and the nucleus was stained with Hoechst 33342 (blue). SCs transfected with siAkr1b8-2 displayed less EdU-positive (red) signal than SCs transfected with siNC. Scale bar: 100 μm. (C) Quantitation of the EdU-positive cells ($n$ = 3). (D, E) Effect of *Akr1b8* knockdown on cell migration in SCs. Wound healing assays are shown in D; both the siAkr1b8-2 group and siNC group displayed no cell migration in the clear area at 0 hours, while the siAkr1b8-2 group showed a slower migration rate than the siNC group at 12 hours and displayed a larger clear area. The quantitation data are shown in E ($n$ = 3). Scale bar: 100 μm. (F, G) Effect of Akr1b8 knockdown on the synthesis of induced chemokines in SCs. The mRNA expression levels of MCP-1 (F) and IL-6 (G) in SCs transfected with siNC or Akr1b8-specific siRNA (siAkr1b8-2, siAkr1b8-3) are shown ($n$ = 3). All data are shown as the mean ± SD. *$P$ < 0.05, **$P$ < 0.01, ***$P$ < 0.001, *vs*. siNC group (Student's $t$-test). IL-6: Interleukin-6; MCP-1: monocyte chemoattractant protein-1; ns: non-significant; SC: Schwann cell; EdU: 5-ethynyl-20-deoxyuridine, siNC: negative-control siRNA.

## Discussion

Our study is the first to reveal transcriptome changes of the facial nerve trunk at the site of crush injury in a facial nerve injury model. Although the facial nerve and sciatic nerve both belong to the PNS, they have different microenvironments, and the gene expression underlying their injury repair differs. Thus, our study facilitates a systematic understanding of peripheral nerve regeneration.

Facial nerve injury results in many cellular and molecular changes in the facial nucleus. Several previous studies involving cDNA microarray analysis have revealed transcriptional alterations of the facial motor nucleus and identified some key genes, such as *Hnt1*, *SRF*, and *ATF3*, that participate in motoneuron regeneration (Zujovic et al., 2005; Stern et al., 2012; Gey et al., 2016). Although microarrays and RNA-seq are both major high-throughput techniques for genome-wide transcriptome profiling, RNA-seq generates a higher nucleotide resolution, can identify transcripts with low abundance that were not previously detected in the target genome, and provide a more precise and comprehensive recognition of transcript expression than microarrays (Gong et

al., 2016). Furthermore, previous microarray analyses of the facial nucleus mainly compared and analyzed the molecular changes of the motoneuron cell body before and after facial nerve injury using only one time point (Zujovic et al., 2005; Stern et al., 2012; Gey et al., 2016). Here, we focused on local damaged axons and analyzed transcriptome changes at continuous time points after nerve injury to provide a dynamic map of gene expression changes in axons at the site of crush injury. The transcriptome changes in axons at the site of crush injury originate from many sources, such as SCs, infiltrating immune cells, and local axonal mRNA transport. Moreover, our RNA-seq analysis detected many differentially expressed SC-derived and infiltrating immune cell-derived genes, e.g., *MCP-1*, *LIF*, *IL-6*, and *IL-1β* (**Additional Table 4**).

In this study, we identified nine new genes that are differentially expressed during facial nerve injury repair. These nine genes have been previously reported to play pivotal roles in cell proliferation, migration, apoptosis, adhesion, and the inflammatory response. These relevant biological processes play important roles in regulating nerve repair, and therefore, we hypothesized that these genes may be involved in the regulation of facial nerve regeneration after injury. To test our hypothesis, we chose *Akr1b8* for further study. Finally, we found that *Akr1b8* knockdown disrupts the synthesis of induced *IL-6* and *MCP-1* in SCs but does not affect SC proliferation and migration, indicating that Akr1b8 regulates facial nerve repair by modulating the interactions between SCs and macrophages after injury. Previous studies have identified 6 hours as a node of nerve regeneration, and many biosynthetic processes related to inflammation were enriched at 6 hours (Li et al., 2015; Yi et al., 2017). Consistently, in our study, *Akr1b8*, *IL-6*, and *MCP-1* were all surprisingly up-regulated to a relatively high level at 6 hours after facial nerve injury (**Additional Table 7**), suggesting a potential correlation among these genes at the initiation of the inflammatory response post-injury and further supporting our opinion. Thus, Akr1b8 may be a potential target to assist in facial nerve injury repair. However, the mechanism by which *Akr1b8* regulates the synthesis of induced cytokines and chemokines requires further investigation.

Additionally, the function of the remaining eight genes, including *C5ar1*, in facial nerve repair is also worthy of further investigation. *C5ar1* is involved in the complement system. The complement system is an innate immune system that is activated within the first hours after injury and plays an essential role in the early inflammatory reactions of Wallerian degeneration, which involves a cascade of inflammatory events alongside injured nerve fibers triggered by axonal degeneration distal to nerve damage (Dubový et al., 2013). *C5ar1* is the most important receptor for the complement component C5a and is widely expressed in inflammatory cells, glial cells, and neurons (Woodruff et al., 2010; Li et al., 2019). Previous studies have confirmed that C5a can inhibit neuron apoptosis and promote microglial phagocytosis, thus protecting neurons in the central nervous system (O'Barr et al., 2001; Rogers et al., 2002; Mukherjee et al., 2008; Guo et al., 2013). However, the roles of C5a and C5ar1 in the PNS have not been elucidated yet. In this study, we found that *C5ar1* expression was up-regulated at 6 hours after facial nerve crush injury, peaked at 4 days, and was down-regulated at 7 days. This trend was completely consistent with previous reports of *C5ar1* after spinal cord injury (Li et al., 2019), suggesting that *C5ar1* has a potential effect on nerve regeneration in the PNS, which deserves further investigation.

Additionally, we identified multiple transcriptional alterations after facial nerve injury by RNA-seq, including not only differential genes but also new long non-coding RNAs (lncRNAs) and circular RNAs (circRNA). As shown in **Additional Table 3**, only approximately 50% of the sequencing reads could be aligned to the reference gene, while lncRNAs and circRNAs accounted for the other 50%. However, in this study, we only analyzed and explored DEGs, and the changes in lncRNAs and circRNAs require further analysis.

This study reveals the transcriptome changes following facial nerve injury and identifies nine genes that may play a role in facial nerve injury repair. However, we have only preliminarily explored the effect of one of these genes, *Akr1b8*, on SCs at the cellular level. Future studies are needed to further explore the potential function of the other eight genes in facial nerve injury repair. Further *in vivo* studies of the effect of Akr1b8 on the SC phenotype and further facial nerve functional estimation following interference with *Akr1b8* expression are needed to verify the role of *Akr1b8* in facial nerve injury repair. However, the mechanism underlying regulation of the expression levels of *MCP-1* and *IL-6* by *Akr1b8* in SCs was revealed in this study and is worth exploring further.

In summary, this is the first study to explore the dynamic changes in differential gene expression at the facial nerve crush site by deep sequencing. Our study offers a new perspective of PNS nerve recovery and identified nine genes that may be critical to promote the initiation of nerve regeneration by regulating cell proliferation, migration, apoptosis, adhesion, or the immunoinflammatory response. These genes may be potential therapeutic targets for facial nerve injury repair.

**Author contributions:** *Study design: LPZ; facial nerve injury model establishment: YS; Schwann cell function analysis: YL; other experimental implementation: SL; gene expression analysis: DW, WF; data analysis and manuscript writing: QQC. All authors approved the final version of the paper.*
**Conflicts of interest:** *The authors declare no conflict of interest.*
**Financial support:** *None.*
**Institutional review board statement:** *This study was approved by Animal Ethics Committee of Nantong University, China (approval No. S20180923-007) in 2018.*
**Copyright license agreement:** *The Copyright License Agreement has been signed by all authors before publication.*
**Data sharing statement:** *Datasets analyzed during the current study are available from the corresponding author on reasonable request.*
**Plagiarism check:** *Checked twice by iThenticate.*
**Peer review:** *Externally peer reviewed.*

**Additional files:**
***Additional Figure 1:*** *Series test of cluster analysis for the sequencing data.*
***Additional Table 1:*** *Lists of primers used in quantitative real-time polymerase chain reaction.*
***Additional Table 2:*** *Summary of the sequencing reads alignment to the reference genome.*
***Additional Table 3:*** *Summary of the sequencing reads alignment to the reference gene.*
***Additional Table 4:*** *The list of differentially expressed genes at different time point post-injury related to Figure 2C.*
***Additional Table 5:*** *The list of enriched Kyoto Encyclopedia of Genes and Genomes pathway for facial nerve tissues.*
***Additional Table 6:*** *The list of genes in Gene Act Network related to Figure 3D.*
***Additional Table 7:*** *The transcriptional alteration of Akr1b8, interleukin 6 (IL-6) and C-C motif chemokine ligand 2 (MCP-1) at different time point post-injury.*

## References

Arumugam P, Suzuki T, Shima K, McCarthy C, Sallese A, Wessendarp M, Ma Y, Meyer J, Black D, Chalk C, Carey B, Lachmann N, Moritz T, Trapnell BC (2019) Long-term safety and efficacy of gene-pulmonary macrophage transplantation therapy of PAP in Csf2ra(-/-) mice. Mol Ther 27:1597-1611.

Aslam Y, Williamson J, Romashova V, Elder E, Krishna B, Wills M, Lehner P, Sinclair J, Poole E (2019) Human cytomegalovirus upregulates expression of HCLS1 resulting in increased cell motility and transendothelial migration during latency. iScience 20:60-72.

Bíró V (2017) Applied methods instead of autologous nerve transplantation in the reconstruction of nerve injuries on the hand. Orv Hetil 158:1163-1167.
Caillaud M, Richard L, Vallat JM, Desmoulière A, Billet F (2019) Peripheral nerve regeneration and intraneural revascularization. Neural Regen Res 14:24-33.
Chan KM, Gordon T, Zochodne DW, Power HA (2014) Improving peripheral nerve regeneration: from molecular mechanisms to potential therapeutic targets. Exp Neurol 261:826-835.
Cho Y, Shin JE, Ewan EE, Oh YM, Pita-Thomas W, Cavalli V (2015) Activating injury-responsive genes with hypoxia enhances axon regeneration through neuronal HIF-1α. Neuron 88:720-734.
Christie KJ, Zochodne D (2013) Peripheral axon regrowth: new molecular approaches. Neuroscience 240:310-324.
da Silva TF, Eira J, Lopes AT, Malheiro AR, Sousa V, Luoma A, Avila RL, Wanders RJ, Just WW, Kirschner DA, Sousa MM, Brites P (2014) Peripheral nervous system plasmalogens regulate Schwann cell differentiation and myelination. J Clin Invest 124:2560-2570.
Dragone LL, Myers MD, White C, Sosinowski T, Weiss A (2006) SRC-like adaptor protein regulates B cell development and function. J Immunol 176:335-345.
Dubový P, Jancalek R, Kubek T (2013) Role of inflammation and cytokines in peripheral nerve regeneration. Int Rev Neurobiol 108:173-206.
Gao D, Tang T, Zhu J, Tang Y, Sun H, Li S (2019) CXCL12 has therapeutic value in facial nerve injury and promotes Schwann cells autophagy and migration via PI3K-AKT-mTOR signal pathway. Int J Biol Macromol 124:460-468.
Gey M, Wanner R, Schilling C, Pedro MT, Sinske D, Knöll B (2016) Atf3 mutant mice show reduced axon regeneration and impaired regeneration-associated gene induction after peripheral nerve injury. Open Biol 6:160091.
Gong L, Wu J, Zhou S, Wang Y, Qin J, Yu B, Gu X, Yao C (2016) Global analysis of transcriptome in dorsal root ganglia following peripheral nerve injury in rats. Biochem Biophys Res Commun 478:206-212.
Guo Q, Cheng J, Zhang J, Su B, Bian C, Lin S, Zhong C (2013) Delayed post-injury administration of C5a improves regeneration and functional recovery after spinal cord injury in mice. Clin Exp Immunol 174:318-325.
Haastert K, Grosheva M, Angelova SK, Guntinas-Lichius O, Skouras E, Michael J, Grothe C, Dunlop SA, Angelov DN (2009) Schwann cells overexpressing FGF-2 alone or combined with manual stimulation do not promote functional recovery after facial nerve injury. J Biomed Biotechnol 2009:408794.
Hadlock TA, Heaton J, Cheney M, Mackinnon SE (2005) Functional recovery after facial and sciatic nerve crush injury in the rat. Arch Facial Plast Surg 7:17-20.
Hamilton MJ, Ho VW, Kuroda E, Ruschmann J, Antignano F, Lam V, Krystal G (2011) Role of SHIP in cancer. Exp Hematol 39:2-13.
He Z, Jin Y (2016) Intrinsic Control of Axon Regeneration. Neuron 90:437-451.
Hu J, Zhou J, Li X, Wang F, Lü H (2011) Schwann cells promote neurite outgrowth of dorsal root ganglion neurons through secretion of nerve growth factor. Indian J Exp Biol 49:177-182.
Kunimura K, Uruno T, Fukui Y (2020) DOCK family proteins: key players in immune surveillance mechanisms. Int Immunol 32:5-15.
Li S, Xue C, Yuan Y, Zhang R, Wang Y, Wang Y, Yu B, Liu J, Ding F, Yang Y, Gu X (2015) The transcriptional landscape of dorsal root ganglia after sciatic nerve transection. Sci Rep 5:16888.
Li Y, Chen Y, Li X, Wu J, Pan JY, Cai RX, Yang RY, Wang XD (2019) RNA sequencing screening of differentially expressed genes after spinal cord injury. Neural Regen Res 14:1583-1593.
Mahar M, Cavalli V (2018) Intrinsic mechanisms of neuronal axon regeneration. Nat Rev Neurosci 19:323-337.
Mao X, Tong J (2018) ARHGAP30 suppressed lung cancer cell proliferation, migration, and invasion through inhibition of the Wnt/β-catenin signaling pathway. Onco Targets Ther 11:7447-7457.
Martini R, Fischer S, López-Vales R, David S (2008) Interactions between Schwann cells and macrophages in injury and inherited demyelinating disease. Glia 56:1566-1577.
Mukherjee P, Thomas S, Pasinetti GM (2008) Complement anaphylatoxin C5a neuroprotects through regulation of glutamate receptor subunit 2 in vitro and in vivo. J Neuroinflammation 5:5.
O'Barr SA, Caguioa J, Gruol D, Perkins G, Ember JA, Hugli T, Cooper NR (2001) Neuronal expression of a functional receptor for the C5a complement activation fragment. J Immunol 166:4154-4162.
Perrin FE, Lacroix S, Avilés-Trigueros M, David S (2005) Involvement of monocyte chemoattractant protein-1, macrophage inflammatory protein-1alpha and interleukin-1beta in Wallerian degeneration. Brain 128:854-866.
Rogers J, Strohmeyer R, Kovelowski CJ, Li R (2002) Microglia and inflammatory mechanisms in the clearance of amyloid beta peptide. Glia 40:260-269.
Rueger MA, Aras S, Guntinas-Lichius O, Neiss WF (2008) Re-activation of atrophic motor Schwann cells after hypoglossal-facial nerve anastomosis. Neurosci Lett 434:253-259.
Shen Y, Ma J, Yan R, Ling H, Li X, Yang W, Gao J, Huang C, Bu Y, Cao Y, He Y, Wan L, Zu X, Liu J, Huang MC, Stenson WF, Liao DF, Cao D (2015) Impaired self-renewal and increased colitis and dysplastic lesions in colonic mucosa of AKR1B8-deficient mice. Clin Cancer Res 21:1466-1476.
Spencer CR, Irving RM (2016) Causes and management of facial nerve palsy. Br J Hosp Med (Lond) 77:686-691.
Stern S, Sinske D, Knöll B (2012) Serum response factor modulates neuron survival during peripheral axon injury. J Neuroinflammation 9:78.
Tofaris GK, Patterson PH, Jessen KR, Mirsky R (2002) Denervated Schwann cells attract macrophages by secretion of leukemia inhibitory factor (LIF) and monocyte chemoattractant protein-1 in a process regulated by interleukin-6 and LIF. J Neurosci 22:6696-6703.
Weng YL, Wang X, An R, Cassin J, Vissers C, Liu Y, Liu Y, Xu T, Wang X, Wong SZH, Joseph J, Dore LC, Dong Q, Zheng W, Jin P, Wu H, Shen B, Zhuang X, He C, Liu K, et al. (2018) Epitranscriptomic m(6)A regulation of axon regeneration in the adult mammalian nervous system. Neuron 97:313-325. e316.
Woodruff TM, Ager RR, Tenner AJ, Noakes PG, Taylor SM (2010) The role of the complement system and the activation fragment C5a in the central nervous system. Neuromolecular Med 12:179-192.
Yao C, Shi X, Zhang Z, Zhou S, Qian T, Wang Y, Ding F, Gu X, Yu B (2016) Hypoxia-induced upregulation of miR-132 promotes Schwann cell migration after sciatic nerve injury by targeting PRKAG3. Mol Neurobiol 53:5129-5139.
Yi S, Tang X, Yu J, Liu J, Ding F, Gu X (2017) Microarray and qPCR analyses of Wallerian degeneration in rat sciatic nerves. Front Cell Neurosci 11:22.
Yu B, Zhou S, Wang Y, Ding G, Ding F, Gu X (2011) Profile of microRNAs following rat sciatic nerve injury by deep sequencing: implication for mechanisms of nerve regeneration. PLoS One 6:e24612.
Zhu H, Zhang L, Wu Y, Dong B, Guo W, Wang M, Yang L, Fan X, Tang Y, Liu N, Lei X, Wu H (2018) T-ALL leukemia stem cell 'stemness' is epigenetically controlled by the master regulator SPI1. Elife 7:e38314.
Zujovic V, Luo D, Baker HV, Lopez MC, Miller KR, Streit WJ, Harrison JK (2005) The facial motor nucleus transcriptional program in response to peripheral nerve injury identifies Hn1 as a regeneration-associated gene. J Neurosci Res 82:581-591.

*C-Editor: Zhao M; S-Editors: Yu J, Li CH; L-Editors: Kreiner L, Frampton RJ, Song LP; T-Editor: Jia Y*

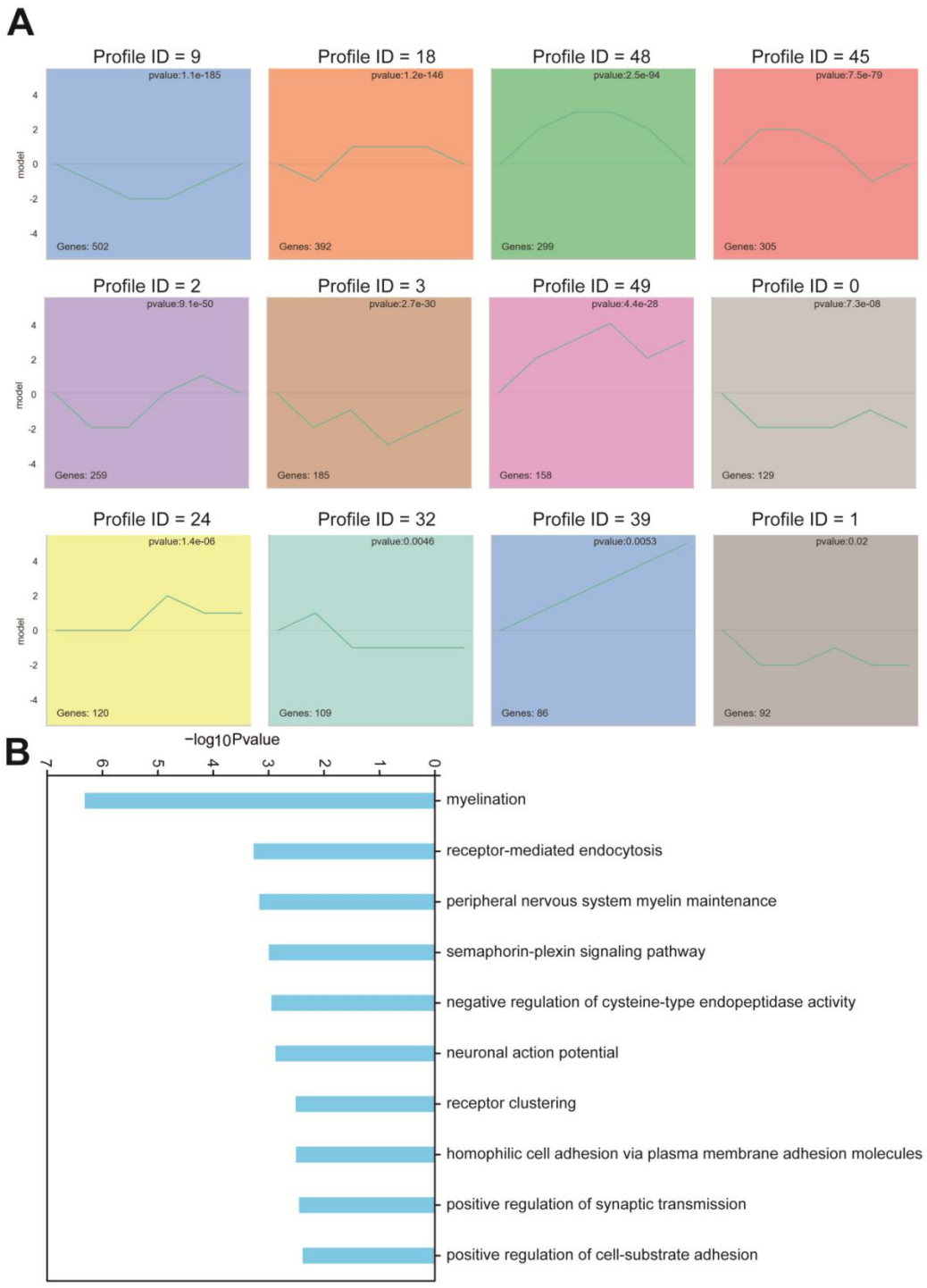


**Additional Figure 1 Series test of cluster analysis for the sequencing data.**

(A) The 12 expression pattern for all detected genes from facial nerve injury segments. Profiles with *P*-value < 0.05 were defined as significant expression patterns. (B) Gene Ontology (GO) enrichment analysis of the biological process for genes in profile 9.

**Additional Table 1 Lists of primers used in quantitative real-time polymerase chain reaction**

| Gene ID | Gene full name | Gene symbol | Primer sequences (5'-3') |
|---|---|---|---|
| 498282 | Rho GTPase activating protein 30 | Arhgap30 | Forward: GGAGTTCCTTATGCGCCACT |
| | | | Reverse: TCTACACCAGCAGAGAGGGAA |
| 286921 | Aldo-keto reductase family 1, member B8 | Akr1b8 | Forward: AGCCCAGGTTCTTATTCGGT |
| | | | Reverse: TCTGCGTCATAGGGAAACTCT |
| 113959 | Complement C5a receptor 1 | C5ar1 | Forward: CCAGGACATGGACCCCATAA |
| | | | Reverse: GGCGTTGACAGTACGTTTGG |
| 652957 | Colony stimulating factor 2 receptor alpha subunit | Csf2ra | Forward: CAACTCGGAGACGCTGAGGAA |
| | | | Reverse: TGTCAGAGATGGAGGATGGGAG |
| 360509 | Dedicator of cytokinesis 2 | Dock2 | Forward: TTCTTCAAGACCATGCTGGC |
| | | | Reverse: ACAGAAGATGCGAGGCTTGT |
| 288077 | Hematopoietic cell specific Lyn substrate 1 | Hcls1 | Forward: GGGCCACGAGTATGTTGCT |
| | | | Reverse: CCCTTGGCATAATCTCGCTGA |
| 54259 | Inositol polyphosphate-5-phosphatase D | Inpp5d | Forward: TGTTCAGGCATCCGAAGGTG |
| | | | Reverse: CGGGGGTTCTCTGTTGGAAG |
| 366126 | Spi-1 proto-oncogene | Spi1 | Forward: ATTGGTGGTGATGGAGACAGC |
| | | | Reverse: GTAGGAAACCTGGTGACTGAGG |
| 338477 | src-like adaptor | Sla | Forward: CACCTGCACCTTTGGAGAGA |
| | | | Reverse: AACAGCCAGCCATGATACACT |
| 24498 | Interleukin 6 | IL-6 | Forward: GTTTCTCTCCGCAAGAGACTT |
| | | | Reverse: ATACTGGTCTGTTGTGGGTGG |
| 24770 | C-C motif chemokine ligand 2 | MCP-1 | Forward: CCACCACTATGCAGGTCTCTG |
| | | | Reverse: GGGGCATTAACTGCATCTGGC |

**Additional Table 2 Summary of the sequencing reads alignment to the reference genome**

| Map to genome | 0 h | | 6 h | | 1d | | 4 d | | 7 d | | 14 d | |
|---|---|---|---|---|---|---|---|---|---|---|---|---|
| | Number | Percentage | Number | Percentage | Number | Percentage | Number | Percentage | Number | Percentage | Number | Percentage |
| Total reads | 94361472 | 100 | 86725114 | 100 | 92982946 | 100 | 89151756 | 100 | 95589746 | 100 | 92713566 | 100 |
| Total mapped reads | 91837375 | 97.33 | 84618445 | 97.57 | 90666413 | 97.51 | 87205806 | 97.82 | 93552894 | 97.87 | 90729701 | 97.86 |
| Multiple mapped | 16293244 | 17.27 | 15040946 | 17.34 | 15689874 | 16.87 | 15530557 | 17.42 | 18288218 | 19.13 | 18091666 | 19.51 |
| Uniquely mapped | 75544131 | 80.06 | 69577499 | 80.23 | 74976539 | 80.63 | 71675249 | 80.40 | 75264676 | 78.74 | 72638035 | 78.35 |
| Read-1 | 37769163 | 40.03 | 34789073 | 40.11 | 37493318 | 40.32 | 35842787 | 40.20 | 37634101 | 39.37 | 36315331 | 39.17 |
| Read-2 | 37774968 | 40.03 | 34788426 | 40.11 | 37483221 | 40.31 | 35832462 | 40.19 | 37630575 | 39.37 | 36322704 | 39.18 |
| Reads map to '+' | 37776834 | 40.03 | 34799926 | 40.13 | 37499420 | 40.33 | 35857880 | 40.22 | 37652840 | 39.39 | 36341257 | 39.20 |
| Reads map to '-' | 37767297 | 40.02 | 34777573 | 40.10 | 37477119 | 40.31 | 35817369 | 40.18 | 37611836 | 39.35 | 36296778 | 39.15 |
| Non-splice reads | 56205991 | 59.56 | 48941713 | 56.43 | 51622868 | 55.52 | 47266712 | 53.02 | 50532165 | 52.86 | 50521705 | 54.49 |
| Splice reads | 19338140 | 20.49 | 20635786 | 23.79 | 23353671 | 25.12 | 24408537 | 27.38 | 24732511 | 25.87 | 22116330 | 23.85 |
| Reads mapped in proper pairs | 73391002 | 77.78 | 67849726 | 78.24 | 73195804 | 78.72 | 69892724 | 78.40 | 73402272 | 76.79 | 70634914 | 76.19 |

**Additional Table 3 Summary of the sequencing reads alignment to the reference gene**

| Map to genome | 0 h | | 6 h | | 1d | | 4 d | | 7 d | | 14 d | |
|---|---|---|---|---|---|---|---|---|---|---|---|---|
| | **Number** | Percentage | Number | Percentage | Number | Percentage | Number | Percentage | Number | Percentage | Number | Percentage |
| Total reads | 94361472 | 100 | 86725114 | 100 | 92982946 | 100 | 89151756 | 100 | 95589746 | 100 | 92713566 | 100 |
| Total mapped reads | 43207477 | 45.79 | 45010663 | 51.90 | 48295739 | 51.94 | 49023279 | 54.99 | 50974637 | 53.33 | 45979621 | 49.59 |
| Multiple mapped | 22267501 | 23.60 | 21707299 | 25.03 | 23637360 | 25.42 | 23701482 | 26.59 | 24760057 | 25.90 | 22564977 | 24.34 |
| Uniquely mapped | 20939976 | 22.19 | 23303364 | 26.87 | 24658379 | 26.52 | 25321797 | 28.40 | 26214580 | 27.42 | 23414644 | 25.25 |
| Read-1 | 10488913 | 11.12 | 11677376 | 13.46 | 12357964 | 13.29 | 12691522 | 14.24 | 13138016 | 13.74 | 11736195 | 12.66 |
| Read-2 | 10451063 | 11.08 | 11625988 | 13.41 | 12300415 | 13.23 | 12630275 | 14.17 | 13076564 | 13.68 | 11678449 | 12.60 |
| Reads map to '+' | 10453900 | 11.08 | 11627840 | 13.41 | 12299091 | 13.23 | 12631239 | 14.17 | 13079248 | 13.68 | 11681343 | 12.60 |
| Reads map to '-' | 10486076 | 11.11 | 11675524 | 13.46 | 12359288 | 13.29 | 12690558 | 14.23 | 13135332 | 13.74 | 11733301 | 12.66 |
| Non-splice reads | 20673577 | 21.91 | 23027365 | 26.55 | 24375921 | 26.22 | 24998089 | 28.04 | 25884212 | 27.08 | 23110175 | 24.93 |
| Splice reads | 266399 | 0.28 | 275999 | 0.32 | 282458 | 0.30 | 323708 | 0.36 | 330368 | 0.35 | 304469 | 0.33 |
| Reads mapped in proper pairs | 20138726 | 21.34 | 22492920 | 25.94 | 23765996 | 25.56 | 24425390 | 27.40 | 25296368 | 26.46 | 22553934 | 24.33 |

**Additional Table 5 The list of enriched Kyoto Encyclopedia of Genes and Genomes pathway for facial nerve tissues**

| ID | Term | ListHits | *P*-value | Enrichment | Genes |
|---|---|---|---|---|---|
| rno05150 | Staphylococcus aureus infection | 5 | 7.29E-09 | 31.84 | C3; C5ar1; Fcgr2a; Itgal; Itgam |
| rno05152 | Tuberculosis | 7 | 3.50E-08 | 12.8091954 | C3; Fcer1g; Fcgr2a; Il10ra; Itgam; Syk; Tlr2 |
| rno05140 | Leishmaniasis | 5 | 4.42E-08 | 23.76119403 | C3; Fcgr2a; Itgam; Ncf2; Tlr2 |
| rno04145 | Phagosome | 7 | 5.64E-08 | 12.04756757 | C3; Fcgr2a; Itgam; Msr1; Ncf2; Olr1; Tlr2 |
| rno04666 | Fc gamma R-mediated phagocytosis | 5 | 2.00E-07 | 18.51162791 | Dock2; Fcgr2a; Inpp5d; Ptprc; Syk |
| rno05134 | Legionellosis | 3 | 2.15E-05 | 17.68888889 | C3; Itgam; Tlr2 |
| rno04380 | Osteoclast differentiation | 4 | 3.24E-05 | 10.43934426 | Fcgr2a; Ncf2; Spi1; Syk |
| rno05169 | Epstein-Barr virus infection | 5 | 4.63E-05 | 7.269406393 | Fgr; Il10ra; Itgal; Spi1; Syk |
| rno04664 | Fc epsilon RI signaling pathway | 3 | 4.78E-05 | 14.47272727 | Fcer1g; Inpp5d; Syk |
| rno04650 | Natural killer cell mediated cytotoxicity | 4 | 5.85E-05 | 9.228985507 | Fcer1g; Fcgr2a; Itgal; Syk |
| rno04072 | Phospholipase D signaling pathway | 4 | 7.91E-05 | 8.663945578 | Cyth4; Fcer1g; Pik3r5; Syk |
| rno04610 | Complement and coagulation cascades | 3 | 0.000106988 | 11.79259259 | C3; C5ar1; Itgam |
| rno05145 | Toxoplasmosis | 3 | 0.000337164 | 8.763302752 | Il10ra; Pik3r5; Tlr2 |
| rno04670 | Leukocyte transendothelial migration | 3 | 0.000386933 | 8.453097345 | Itgal; Itgam; Ncf2 |
| rno04611 | Platelet activation | 3 | 0.00056779 | 7.6416 | Fcer1g; Pik3r5; Syk |
| rno04514 | Cell adhesion molecules (CAMs) | 3 | 0.001750456 | 5.652071006 | Itgal; Itgam; Ptprc |
| rno05167 | Kaposi's sarcoma-associated herpesvirus infection | 3 | 0.003596227 | 4.636893204 | C3; Pik3r5; Syk |
| rno04060 | Cytokine-cytokine receptor interaction | 3 | 0.0064672 | 3.930864198 | Csf2ra; Il10ra; Tnfrsf1b |
| rno04151 | PI3K-Akt signaling pathway | 3 | 0.019935555 | 2.826035503 | C3; C5ar1; Fcgr2a; Itgal; Itgam |

**Additional Table 6 The list of genes in Gene Act Network related to Figure 3D**

| SUID | Average shortest path length | Betweenness centrality | Closeness centrality | Clustering coefficient | Degree | Name | Neighborhood connectivity | Number of directed edges | Number of undirected edges | Self loops | Topological coefficient |
|---|---|---|---|---|---|---|---|---|---|---|---|
| 103 | 2.294118 | 0.082105 | 0.435897 | 0.625 | 16 | Lcp1 | 11.6875 | 16 | 0 | 0 | 0.486979 |
| 102 | 2.176471 | 0.074734 | 0.459459 | 0.685714 | 15 | Hcls1 | 11.8 | 15 | 0 | 0 | 0.561905 |
| 99 | 2.205882 | 0.054851 | 0.453333 | 0.747253 | 14 | Fcgr2a | 12.14286 | 14 | 0 | 0 | 0.578231 |
| 105 | 2.205882 | 0.058092 | 0.453333 | 0.703297 | 14 | Arhgap30 | 11.78571 | 14 | 0 | 0 | 0.561224 |
| 86 | 2.382353 | 0.121733 | 0.419753 | 0.564103 | 13 | Mafb | 11.69231 | 13 | 0 | 0 | 0.487179 |
| 101 | 2.205882 | 0.064208 | 0.453333 | 0.75641 | 13 | Inpp5d | 12.30769 | 13 | 0 | 0 | 0.559441 |
| 106 | 2.235294 | 0.034031 | 0.447368 | 0.820513 | 13 | Ptprc | 12.38462 | 13 | 0 | 0 | 0.589744 |
| 96 | 2.352941 | 0.054286 | 0.425 | 0.757576 | 12 | Sla | 11.66667 | 12 | 0 | 0 | 0.614035 |
| 109 | 2.529412 | 0.003537 | 0.395349 | 0.878788 | 12 | Csf2ra | 12.83333 | 12 | 0 | 0 | 0.641667 |
| 110 | 2.529412 | 0.003537 | 0.395349 | 0.878788 | 12 | Spi1 | 12.83333 | 12 | 0 | 0 | 0.641667 |
| 95 | 2.647059 | 0.019753 | 0.377778 | 0.818182 | 11 | LOC108348047 | 12.09091 | 11 | 0 | 0 | 0.671717 |
| 100 | 2.294118 | 0.052969 | 0.435897 | 0.781818 | 11 | LOC103693389 | 12.63636 | 11 | 0 | 0 | 0.601732 |
| 92 | 2.617647 | 0.003489 | 0.382022 | 0.866667 | 10 | Akr1b8 | 12.7 | 10 | 0 | 0 | 0.668421 |
| 97 | 2.470588 | 0.058319 | 0.404762 | 0.577778 | 10 | C5ar1 | 11.6 | 10 | 0 | 0 | 0.483333 |
| 107 | 2.764706 | 0.093806 | 0.361702 | 0.533333 | 10 | Fcer1g | 9 | 10 | 0 | 0 | 0.391304 |
| 108 | 2.852941 | 0.079834 | 0.350515 | 0.533333 | 10 | Dock2 | 7.9 | 10 | 0 | 0 | 0.37619 |
| 82 | 2.5 | 0.082591 | 0.4 | 0.5 | 9 | Nfam1 | 10.22222 | 9 | 0 | 0 | 0.439614 |
| 80 | 2.352941 | 0.401372 | 0.425 | 0.714286 | 8 | Il10ra | 11.875 | 8 | 0 | 0 | 0.618421 |
| 98 | 2.529412 | 0.03347 | 0.395349 | 0.607143 | 8 | Msr1 | 11.75 | 8 | 0 | 0 | 0.489583 |
| 104 | 3 | 0.033717 | 0.333333 | 0.666667 | 7 | Bin2 | 8.571429 | 7 | 0 | 0 | 0.451128 |
| 88 | 3.558824 | 0.001037 | 0.280992 | 0.866667 | 6 | Ninj1 | 7.166667 | 6 | 0 | 0 | 0.651515 |
| 89 | 3.558824 | 0.001037 | 0.280992 | 0.866667 | 6 | Itgal | 7.166667 | 6 | 0 | 0 | 0.651515 |
| 79 | 3.588235 | 6.81E-04 | 0.278689 | 0.9 | 5 | Syk | 7.4 | 5 | 0 | 0 | 0.672727 |
| 87 | 3.705882 | 3.57E-04 | 0.269841 | 0.9 | 5 | Myo1f | 6.8 | 5 | 0 | 0 | 0.68 |
| 91 | 4.235294 | 0.052882 | 0.236111 | 0.3 | 5 | Pik3r5 | 3.4 | 5 | 0 | 0 | 0.425 |
| 83 | 4.294118 | 0.07041 | 0.232877 | 0.5 | 4 | Ncf2 | 3.25 | 4 | 0 | 0 | 0.464286 |
| 94 | 3.529412 | 0.141117 | 0.283333 | 0.333333 | 4 | Tnfrsf1b | 3.25 | 4 | 0 | 0 | 0.428571 |
| 78 | 2.852941 | 0.372252 | 0.350515 | 0 | 3 | Itgam | 5 | 3 | 0 | 0 | 0.363636 |
| 84 | 5.117647 | 0.003565 | 0.195402 | 0.666667 | 3 | C3 | 3.666667 | 3 | 0 | 0 | 0.611111 |
| 90 | 3.558824 | 0.152406 | 0.280992 | 0.333333 | 3 | Atp8b4 | 4 | 3 | 0 | 0 | 0.52381 |
| 93 | 4.323529 | 0.004159 | 0.231293 | 0.666667 | 3 | Fgr | 3.666667 | 3 | 0 | 0 | 0.52381 |
| 76 | 4.470588 | 0 | 0.223684 | 1 | 2 | Slpi | 3.5 | 2 | 0 | 0 | 0.875 |
| 77 | 3.294118 | 0 | 0.303571 | 1 | 2 | Snx20 | 11.5 | 2 | 0 | 0 | 0.958333 |
| 85 | 5.235294 | 0 | 0.191011 | 1 | 2 | Tlr2 | 3.5 | 2 | 0 | 0 | 0.875 |
| 81 | 3.470588 | 0 | 0.288136 | 0 | 1 | Cyth4 | 9 | 1 | 0 | 0 | 0 |

**Additional Table 7 The transcriptional alteration of Akr1b8, interleukin 6 (IL-6) and C-C motif chemokine ligand 2 (MCP-1) at different time point post-injury**

| Genes | 6 h | 1 d | 4 d | 7 d | 14 d |
|---|---|---|---|---|---|
| Akr1b8 | 14.56112375 | 15.56309085 | 12.8832167998478 | 4.50589301413075 | 3.66420027936358 |
| IL-6 | 208.34055865512 | 0 | 0 | 0 | 0.04677361668083 78 |
| MCP-1 | 126.453695676449 | 30.4586381 | 14.8116965105601 | 0 | 0 |

Date are expressed as fold change (*vs*. 0 hour).